JMEPEG (2009) 18:1140–1143
DOI: 10.1007/s11665-008-9346-x

1059-9495/$19.00

Preparation and Thermal Conductivity of $Sm_2(Zr_{0.6}Ce_{0.4})_2O_7$ Ceramic

Hong-song Zhang, Kun Sun, Qiang Xu, Fu-chi Wang, and Ling Liu

(Submitted March 17, 2008; in revised form October 25, 2008)

A pure $Sm_2(Zr_{0.6}Ce_{0.4})_2O_7$ ceramic was prepared via solid-state reaction using ZrO_2, CeO_2, and Sm_2O_3 as the starting powders at 1600 °C for 10 h. The phase composition and microstructure were studied by X-ray diffraction (XRD), Fourier-transform infrared spectrometer (FT-IR), and scanning electron microscope (SEM). The thermal conductivity was measured by laser-flash method. The results indicated that the prepared ceramic had a pure fluorite structure. Its microstructure was dense with a relative density of 93.35% and there were no other unreacted oxides or interphases in the interfaces between grains. Because of the structure transformation from pyrochlore to fluorite, the synthesized product had a higher thermal conductivity than $Sm_2Zr_2O_7$ ceramic. However, the average thermal conductivity of $Sm_2(Zr_{0.6}Ce_{0.3})_2O_7$ was lower than that of yttria-stabilized zirconia. The measurements of thermal conductivity suggested that the synthesized ceramic can be used as a new material for new thermal barrier coatings in the future.

Keywords ceramics, rare earth zirconate, thermal barrier coatings, thermal conductivity

1. Introduction

Thermal barrier coatings (TBCs) made of low-thermal conductivity ceramics have been used to protect the key metallic components, such as turbine blades and combustors, from the hot gas stream in advanced gas-turbine and diesel engines (Ref 1). Thermal barrier coatings are material system consisting of a thermally insulated ceramic layer and a metallic bond-coat layer. The bond coat provides oxidation protection to the substrate material and reduces the difference in thermal expansion between the substrate and the ceramic layer (Ref 2). Therefore, effective TBCs should exhibit low thermal conductivity, strong adherence to the substrate, phase stability, and thermal shock resistance during thermal cycling, and provide oxidation and corrosion protection to both the metallic bond coat and the substrate (Ref 3). Low thermal conductivity is the most critical requirement for ceramic material for TBCs (Ref 4). TBCs based on 6-8 mol% yttria-stabilized zirconia (YSZ) have been widely used, owing to their low thermal conductivity, good chemical and thermal stability, relatively high coefficient of thermal expansion (relative to the metallic substrate), and high resistance to spalt under thermal fatigue (Ref 5). However, engine temperatures are expected to continue to increase as higher-efficiency engines having higher power-to-weight ratios are designed. Nowadays, the main turbine-producing manufacturers provide an initial gas temperature level of 960-1100 °C for basic service and 1065-1300 °C for peak service. In military aircraft turbines, the temperature of the gas rises to 1600+°C and for commercial aircraft up to 1500+°C (Ref 6). To meet this ambitious goal, the most feasible and economic method is searched for alternatives to YSZ (Ref 7). In part, this is because the YSZ currently used comprise t-prime (t′) zirconia that, being metastable, becomes increasingly unstable at higher temperatures, decomposing to a mixture of tetragonal and cubic zirconia. On cooling, the tetragonal phase transforms to monoclinic zirconia, a disruptive transformation. In part, also, the recent demonstration indicates that the rare earth zirconates with the type of $Ln_2Zr_2O_7$ have lower thermal conductivity than YSZ, which has also spurred a fresh examination of the prospects for discovering alternative materials for thermal barrier coating.

Several interesting zirconates such as $La_2Zr_2O_7$, $Gd_2Zr_2O_7$, $Dy_2Zr_2O_7$, $Nd_2Zr_2O_7$, and $Sm_2Zr_2O_7$ have been investigated (Ref 7, 8). However, the current research is mainly focused on single rare earth zirconates, and research on the doped zirconates on B site has not been attempted on up to now. In this paper, the $Sm_2(Zr_{0.6}Ce_{0.4})_2O_7$ ceramic was prepared by a solid-state reaction method and the thermal conductivity was examined.

2. Experimental

Samples of $Sm_2(Zr_{0.6}Ce_{0.4})_2O_7$ were synthesized by means of a solid-state reaction, using CeO_2 (Rare-Chem Hi-Tech Co., Ltd, purity ≥99.99%), Sm_2O_3 (Rare-Chem Hi-Tech, Co., Ltd, purity ≥99.99%), and ZrO_2 (Farmeiya Advanced Materials Co., Ltd), purity ≥99.9%, including 2.57% HfO_2 as the starting material.

The weighted powers were wet ball-milled for 6 h, using a milling pot made of synthetic resin and resin-coated balls whose

Hong-song Zhang, Department of Mechanical and Electrical Engineering, Henan Institute of Engineering, Zhengzhou, Henan 450007, China; **Kun Sun**, Department of Physics and Electronics, Chuxiong Normal University, Chuxiong, Yunnan 675000, China; and **Qiang Xu, Fu-chi Wang,** and **Ling Liu**, School of Materials Science and Engineering, Beijing Institute of Technology, Beijing 100081, China. Contact e-mail: zhs761128@163.com.

diameter were 2, 4, 6, and 8 mm, respectively, and ethanol as the dispersion reagent. After drying, the powder mixtures were calcined at 800 °C for 5 h in air. After sieving under 53 μm in mesh size, the powders were uniaxially cold pressed into pellets under 100 MPa pressure. The pellets were placed on zirconia tiles and sintered at 1600 °C for 10 h. The pellets were subsequently cooled in air from 1600 °C in the end.

Phase composition analysis of the synthesized sample was determined by X-ray diffractometry (XRD, X'Pert PRD MPD Holand) with Ni-filtered CuKα radiation (0.1542 nm) at the scanning rate of 4°/min. The morphology of polished and thermally etched cross-sections was examined using scanning electron microscope (SEM, HITACHI S-3500). The infrared spectrum was recorded using Nicolet Magna-IR 750 Fourier-transform spectrometer at room temperature.

The thermal diffusivity (λ) of synthesized sample was measured using laser-flash method (Model NETZSCH LFA 427, Germany) in the range between ambient and 1200 °C in an argon atmosphere. The sample dimension for thermal diffusivity measurement was about 10 mm in diameter and about 1 mm in thickness. Before thermal diffusivity measurement, both the front and back faces of the specimens were coated with a thin layer of graphite. These coatings were done to prevent direct transmission of laser beam through the translucent specimens. The thermal diffusivity measurement of the specimens was conducted three times at 20, 200, 400, 600, 800, 1000, and 1200 °C and the average value of thermal diffusivities were recorded. Values for the specific heat capacity (C_p), in the range from ambient to 1200 °C, were calculated using the method in Ref 9 and 10. The thermal conductivities (k) of the specimens were given by Eq 1 with specific heat capacity (C_p), density (ρ), and thermal diffusivity (λ).

$$k = \lambda \cdot \rho \cdot C_p \qquad \text{(Eq 1)}$$

Because the sintered specimens were not full dense, the measured values of thermal conductivities were modified for the actual value k_0 using Eq 2,

$$\frac{k}{k_0} = 1 - \frac{4}{3}\phi, \qquad \text{(Eq 2)}$$

where ϕ is the fractional porosity and the coefficient 4/3 is used to eliminate the effect of porosity on actual thermal conductivity.

3. Results and Discussion

3.1 XRD Pattern and FT-IR Spectra

The XRD patterns of $Sm_2(Zr_{0.6}Ce_{0.4})_2O_7$ and $Sm_2Zr_2O_7$ prepared by solid-state reaction are shown in Fig. 1. It can be seen that the XRD pattern of $Sm_2(Zr_{0.6}Ce_{0.4})_2O_7$ resembles that of $Sm_2Zr_2O_7$ and no other phases exist in the product. In contrast to $Sm_2(Zr_{0.6}Ce_{0.4})_2O_7$, $Sm_2Zr_2O_7$ has two additional peaks at 2θ = 37.4° and 44.6° (indicated as "◇" symbol in Fig. 1). These two peaks can help us distinguish the fluorite and the pyrochlore structures (Ref 11, 12). The XRD results show that a pure $Sm_2(Zr_{0.6}Ce_{0.4})_2O_7$ ceramic with fluorite structure is synthesized in this research. The earlier research results revealed that the ionic radius ratio, RR = (r_A^{3+}/r_B^{4+}) of rare earth zirconates of the type $Ln_2Zr_2O_7$, and the oxygen parameter (x) govern the formation and stability of the pyrochlore oxides.

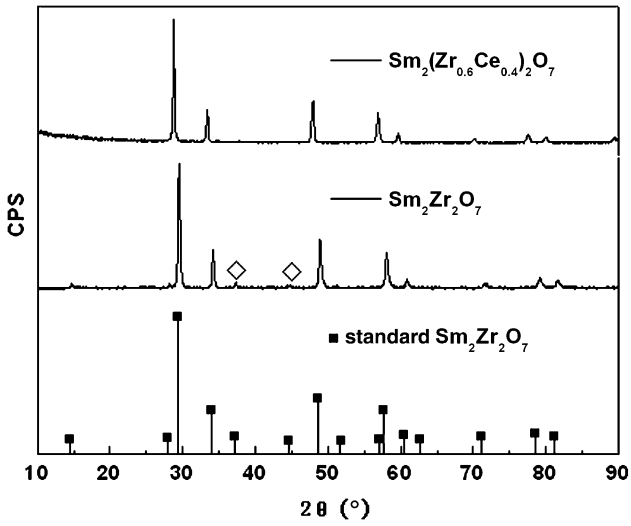

Fig. 1 XRD patterns of $Sm_2(Zr_{0.6}Ce_{0.4})_2O_7$ and $Sm_2Zr_2O_7$

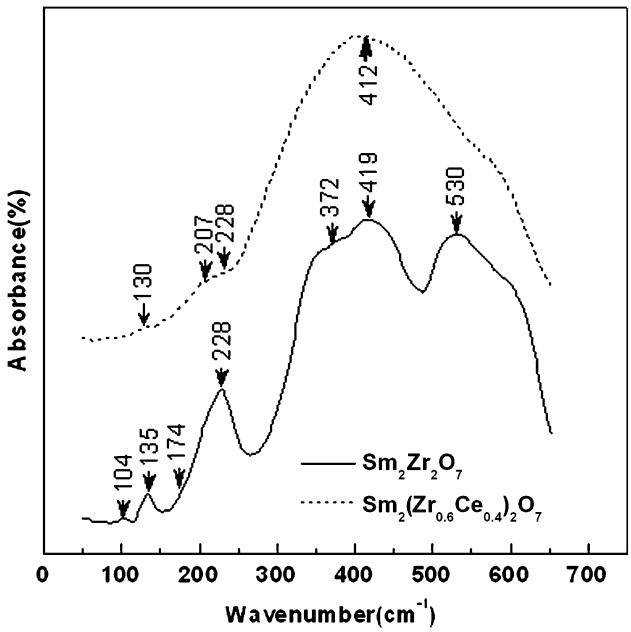

Fig. 2 FT-IR spectra of $Sm_2(Zr_{0.6}Ce_{0.4})_2O_7$ and $Sm_2Zr_2O_7$

A stable pyrochlore oxides can form for RR = 1.46 to 1.78 at one atmosphere pressure, and fluorite oxides will form if RR is lower than 1.46 (Ref 13). Because the Ce^{4+} ion radius (0.97 Å) is greater than that of Zr^{4+} ion (0.72 Å), substituting Ce^{4+} ions for Zr^{4+} ions in $Sm_2Zr_2O_7$ lattice partially will reduce the ionic radius ratio. The RR of $Sm_2(Zr_{0.6}Ce_{0.4})_2O_7$ is only 1.317 which is lower than that of $Sm_2Zr_2O_7$ (1.50). The increase of ion radius at B site in $Sm_2Zr_2O_7$ lattice leads to the formation of fluorite structure. In the meantime, substituting Ce^{4+} ions for Zr^{4+} moves $Sm_2(Zr_{0.6}Ce_{0.4})_2O_7$ diffraction peaks to relatively lower angles.

Besides XRD patterns, the crystal structure of $Sm_2(Zr_{0.6}Ce_{0.4})_2O_7$ can also be reflected by infrared spectra presented in Fig. 2. It can be seen from Fig. 2 that there are seven obvious infrared lattice vibration frequencies in infrared spectra of $Sm_2Zr_2O_7$. This is the typical feature of infrared spectra of zirconate pyrochlore spectra (Ref 13). However, the

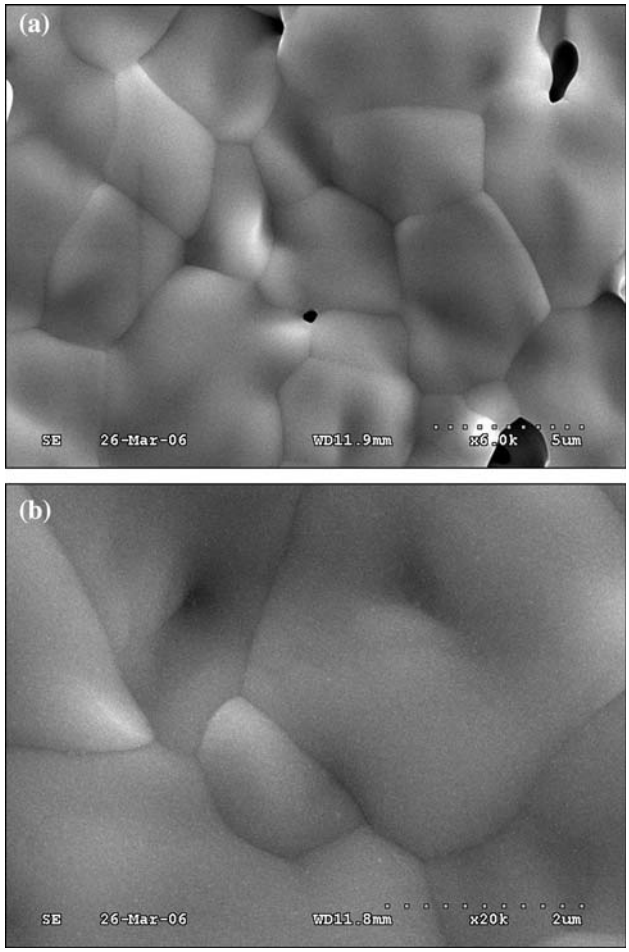

Fig. 3 Microstructure of $Sm_2(Zr_{0.6}Ce_{0.4})_2O_7$ ceramic

infrared lattice vibration frequencies at 412 cm^{-1} broadened apparently as compared to that of $Sm_2Zr_2O_7$, and the presence of substituted cation is the cause of the peak broadening at 412 cm^{-1} (Ref 14).

3.2 SEM

Figure 3 shows the typical microstructure of $Sm_2(Zr_{0.6}Ce_{0.4})_2O_7$ prepared by solid-state synthesis. As can be seen from Fig. 3(a), the microstructure of the synthesized product was dense, but some apparent pores were found. The relative density of the product measured accurately by using Archimedes method is 93.35%. Figure 3(b) shows a high-magnification scanning electron micrograph of the $Sm_2(Zr_{0.6}Ce_{0.4})_2O_7$ ceramic. It is observed that the interfaces between $Sm_2(Zr_{0.6}Ce_{0.4})_2O_7$ particles are very clean and no other interphases or unrecated oxides exist in the interfaces, as shown in Fig. 3(b).

3.3 Thermal Conductivity

The diffusivity of $Sm_2(Zr_{0.6}Ce_{0.4})_2O_7$ decreases with an increase of temperature in the range between ambient and 1200 °C (Fig. 4). Figure 4 shows an inverse temperature dependence, i.e., $\lambda \propto T^{-1}$, in this temperature range. The T^{-1} dependence of diffusivity for $Sm_2(Zr_{0.6}Ce_{0.4})_2O_7$ suggests a dominant phonon conduction behavior, which resembles most polycrystalline materials (Ref 7).

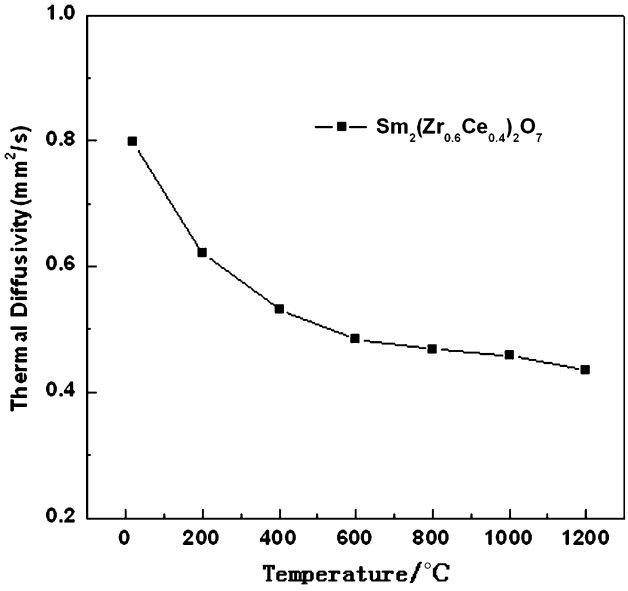

Fig. 4 Thermal diffusivity of $Sm_2(Zr_{0.6}Ce_{0.4})_2O_7$

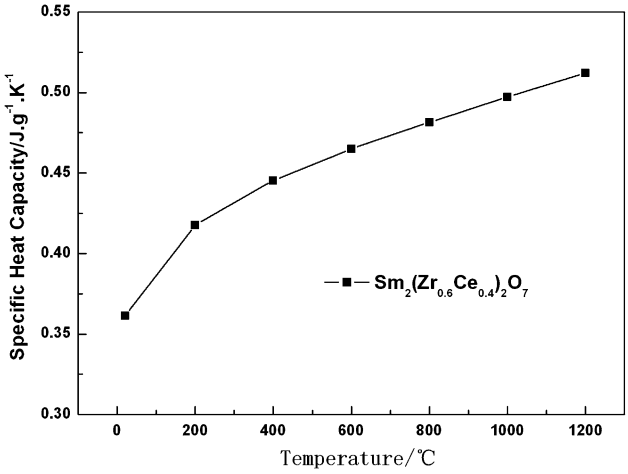

Fig. 5 Specific heat capacity of $Sm_2(Zr_{0.6}Ce_{0.4})_2O_7$

The specific heat of $Sm_2(Zr_{0.6}Ce_{0.4})_2O_7$ at various temperatures is illustrated in Fig. 5, which lists nearly a linear temperature dependence, i.e.,$C_p \propto T$. Because of the limitation of the measurement apparatus, the specific heat capacity can be fitted as the following equation in this temperature range according to the calculation method explained in Ref 9 and 10.

$$C_p = 0.41184 + 0.7 \times 10^{-4} \times T - 6099.35631 \times T^{-2} \quad \text{(Eq 3)}$$

The values of thermal conductivity are thus obtained by multiplying the thermal diffusivity, density, and specific heat capacity according to Eq 3 and are plotted in Fig. 6. It can be seen that thermal conductivity of $Sm_2(Zr_{0.6}Ce_{0.4})_2O_7$ and $Sm_2Zr_2O_7$ decreases gradually with increasing temperature. The value of thermal conductivity of $Sm_2(Zr_{0.6}Ce_{0.4})_2O_7$ decreases from 1.96 to 1.52 W/m K in this temperature range. The thermal conductivity of $Sm_2(Zr_{0.6}Ce_{0.4})_2O_7$ is higher than that of $Sm_2Zr_2O_7$.

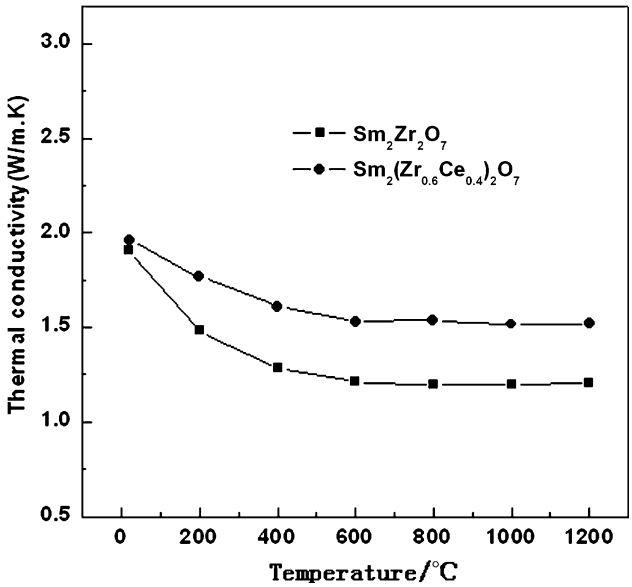

Fig. 6 Thermal conductivity of $Sm_2(Zr_{0.6}Ce_{0.4})_2O_7$ and $Sm_2Zr_2O_7$

It is well known that a substitutional solid solution is formed by the substitution of Zr^{4+} ions by Ce^{4+} ions when CeO_2 is doped into $Sm_2Zr_2O_7$ (Ref 7). According to the phonon heat conduction theory, substituting Ce^{4+} ions for Zr^{4+} ions will reduce the phonon average mean free path because of the difference in mass and ion radius between Ce^{4+} ion and Zr^{4+} ion. So the thermal conductivity of $Sm_2(Zr_{0.6}Ce_{0.4})_2O_7$ should be lower than that of $Sm_2Zr_2O_7$. However, the experimental results of thermal conductivity suggest just the reverse. The higher thermal conductivity of $Sm_2(Zr_{0.6}Ce_{0.4})_2O_7$ can be attributed to the transformation of crystal structure. In disordered fluorite structure, the formation probability of ion vacancy groups or pairs is greater than pyrochlore structure (Ref 15). The vacancies constituting groups or pairs have no effect on phonon scattering, so the substitution of Zr^{4+} ions by Ce^{4+} ions when CeO_2 is doped into $Sm_2Zr_2O_7$ can not decrease the average mean free path of phonons. With the crystal structure transformation from $Sm_2Zr_2O_7$ to $Sm_2(Zr_{0.6}Ce_{0.4})_2O_7$, the increased average free path leads to the higher thermal conductivity of $Sm_2(Zr_{0.6}Ce_{0.4})_2O_7$. Despite the fact that $Sm_2(Zr_{0.6}Ce_{0.4})_2O_7$ has higher thermal conductivity than $Sm_2Zr_2O_7$, the average values of the thermal conductivity $Sm_2(Zr_{0.6}Ce_{0.4})_2O_7$ in the range between ambient and 1200 °C is only 1.62 W/m K, which is lower than 2.5 W/m K (Ref 7), the average value of 8YSZ thermal conductivity.

As is well known, lower thermal conductivity is the most critical requirements of ceramic material for TBCs. The average thermal conductivity of current 8YSZ is much higher than that of $Sm_2(Zr_{0.6}Ce_{0.4})_2O_7$. So the thermal conductivity of $Sm_2(Zr_{0.6}Ce_{0.4})_2O_7$ fulfills the basic requirement of ceramic material for TBCs.

4. Conclusions

1. $Sm_2(Zr_{0.6}Ce_{0.4})_2O_7$ ceramic material with fluorite crystal structure can be prepared successfully by a solid-state reaction using ZrO_2, Sm_2O_3, and CeO_2 as starting powders at 1600 °C for 10 h.
2. The thermal conductivity of $Sm_2(Zr_{0.6}Ce_{0.4})_2O_7$ is lower than that of YSZ, so the thermal conductivity satisfies the basic requirement of new TBCs. $Sm_2(Zr_{0.6}Ce_{0.4})_2O_7$ can be explored as a new prospective candidate material for use in new TBC systems.
3. The higher thermal conductivity of $Sm_2(Zr_{0.6}Ce_{0.4})_2O_7$ as compared to $Sm_2Zr_2O_7$ can be attributed to the crystal structure transformation from pyrochlore to fluorite. The effect of structure transformation on phonon scattering exceeds that of increasing of atomic weight and crystal lattice aberrance.

Acknowledgments

This work is supported by the Excellent Young Scholars Research Fund of Beijing Institute of Technology (No. 2006Y0409) and the Commission of Science Technology and Industry for National Defense (No. 9140A1202030BQ0102).

References

1. N.P. Padture, G. Maurice, and H.E. Jordan, Thermal Barrier Coatings for Gas-Turbine Engine Applications, *Science*, 2002, **12**, p 280–284
2. F. Martin, P. Christer, and J. Wigren, Influence of Particle In-Flight Characteristics on the Microstructure of Atmospheric Plasma Sprayed Yttria Stabilized ZrO_2, *Surf. Coat. Technol.*, 2001, **141**, p 115–127
3. J.F. Li, H.L. Liao, C.X. Ding, and C. Coddet, Optimizing the Plasma Spray Process Parameters of Yttria Stabilized Zirconia Coatings Using Uniform Design of Experiments, *J. Mater. Process. Technol.*, 2005, **160**, p 34–42
4. A. Kulkarni, A. Vaidya, A. Goland, S. Sampath, and H. Herman, Processing Effects on Porosity-Property Correlations in Plasma Yttria-Stabilized Zirconia Coatings, *Mater. Sci. Eng.*, 2003, **A359**, p 100–111
5. X.Q. Cao, R. Vassen, and D. Stoever, Ceramic Materials for Thermal Barrier Coatings, *J. Eur. Ceram. Soc.*, 2004, **24**, p 1–10
6. W. Beele, G. Marijnissen, and A.V. Lieshout, The Evolution of Thermal Barrier Coatings—Status and Upcoming Solutions for Today's Key Issues, *Surf. Coat. Technol.*, 1999, **120–121**, p 61–67
7. X. Qiang, P. Wei, W.J. Dong, Q.L. Hao, M.H. Zhuo, K. Mori, and T. Torigoe, Preparation and Thermophysical Properties of $Dy_2Zr_2O_7$ Ceramic for Thermal Barrier Coatings, *Mater. Lett.*, 2005, **59**, p 2804–2807
8. D.R. Clarke, Materials Selection Guidelines for Low Thermal Conductivity Thermal Barrier Coatings, *Surf. Coat. Technol.*, 2003, **163–164**, p 67–74
9. P.G. Spencer, Estimation of Thermodynamic Data for Metallurgical Applications, *Thermochim. Acta*, 1998, **314**, p 1–21
10. J.D. Leitner, P. Chuchvalec, and D. Sedmidubsky, Estimation of Heat Capacity of Solid Mixed Oxides, *Thermochim. Acta*, 2003, **395**, p 27–46
11. S.J. Patwe, B.R. Amberkar, and A.K. Tyagi, Synthesis, Characterization and Lattice Thermal Expansion of Some Compounds in the System $Gd_2Ce_xZr_{2-x}O_7$, *J. Alloys Compd.*, 2005, **389**, p 243–246
12. C.X. Qiang, R. Vassen, and W. Fishher, Lanthanum-Cerium Oxides as a Thermal Barrier-Coating Materials for High-Temperature Applications, *Adv. Mater.*, 2003, **15**, p 1438–1442
13. M.A. Subramanian, G. Aravamudan, and G.V. Subba Rao, Oxides pyrochlore—a review, *Prog. Solid State Chem.*, 1983, **15**, p 55–143
14. T.K. Kang, T. Nagasaki, and N. Igawa, Electrical Properties of Cubic, Stabilized, Single ZrO_2-Gd_2O_3 Crystals, *J. Am. Ceram. Soc.*, 1992, **8**, p 2297–2299
15. B.E. Scheetz and W.B. White, Characterization of Anion Disorder in Zirconate $A_2B_2O_7$ Compounds by Raman Spectroscopy, *J. Am. Ceram. Soc.*, 1979, **9–10**, p 468–470